Hindawi
Geofluids
Volume 2018, Article ID 7321961, 14 pages
https://doi.org/10.1155/2018/7321961

Research Article

A Damage Constitutive Model for the Effects of CO_2-Brine-Rock Interactions on the Brittleness of a Low-Clay Shale

Qiao Lyu,[1,2] Xinping Long,[3] P. G. Ranjith,[4] Jingqiang Tan,[1,2] Yong Kang,[3] and Wenbin Luo[1,2]

[1]*Key Laboratory of Metallogenic Prediction of Nonferrous Metals and Geological Environment Monitoring, Ministry of Education, Central South University, Changsha 410083, China*
[2]*School of Geosciences and Info-physics, Central South University, Changsha 410083, China*
[3]*Key Laboratory of Hubei Province for Water Jet Theory & New Technology, Wuhan University, Wuhan 430072, China*
[4]*Deep Earth Energy Lab, Department of Civil Engineering, Monash University, Melbourne 3800, Australia*

Correspondence should be addressed to Jingqiang Tan; tanjingqiang@gmail.com

Received 14 November 2017; Revised 24 February 2018; Accepted 25 March 2018; Published 30 May 2018

Academic Editor: Julie K. Pearce

CO_2 is a very promising fluid for drilling and nonaqueous fracturing, especially for CO_2-enhanced shale gas recovery. Brittleness is a very important characteristic to evaluate the drillability and fracability. However, there is not much relevant research works on the influence of CO_2 and CO_2-based fluids on shale's brittleness been carried out. Therefore, a series of strength tests were conducted to obtain the stress-strain characteristics of shale soaked in different phases of CO_2 including subcritical or supercritical CO_2 with formation of water for different time intervals (10 days, 20 days, and 30 days). Two damage constitutive equations based on the power function distribution and Weibull distribution were established to predict the threshold stress for both intact and soaked shale samples. Based on the results, physical and chemical reactions during the imbibition cause reductions of shales' peak axial strength (20.79%~61.52%) and Young's modulus (13.14%~62.44%). Weibull distribution-based constitutive model with a damage threshold value of 0.8 has better agreement with the experiments than that of the power function distribution-based constitutive model. The energy balance method together with the Weibull distribution-based constitutive model is applied to calculate the brittleness values of samples with or without soaking. The intact shale sample has the highest BI value of 0.9961, which is in accordance with the high percentage of brittleness minerals of the shale samples. The CO_2-NaCl-shale interactions during the imbibition decrease the brittleness values. Among the three soaking durations, the minimum brittleness values occur on samples with 20 days' imbibition in subcritical and supercritical CO_2 + NaCl solutions and the reductions of which are 2.08% and 2.49%, respectively. Subcritical/supercritical CO_2 + NaCl imbibition has higher effect on shale's strength and Young's modulus than on the brittleness. The low-clay shale still keeps good fracture performance after imbibition.

1. Introduction

The increasing trend of greenhouse gas emissions contributes significantly to global warming. CO_2 (carbon dioxide), one of the main greenhouse gases, has been investigated by many researchers which aim to reduce its concentration by means of CCUS (CO_2 capture, utilization, and sequestration) project [1–5]. Because of the unique properties, CO_2 presents a great feasibility in the utilizations of drilling industry [6, 7] and nonaqueous fracking for shale gas recovery [8–10]. During the drilling and fracturing process, CO_2 together with ground water or other fluids will interact with rock and change rock's mechanical properties [11–14].

Shale is a kind of a compacted sedimentary rock which accounts for 75% of drilled formations [15]. Therefore, the investigation of shale's mechanical properties after fluid-rock interactions is very important for drilling and fracturing industry. Many scholars have done a brilliant research about the variation of shale's strength and Young's modulus after the adsorption of fluids, such as water [16, 17], saline solutions [18, 19], CO_2 [20–22], CO_2-dissolved water [11], and

CO_2-dissolved brine [23, 24]. However, the studies of the brittleness of shale after fluid saturation are limited. As brittleness is a very important mechanical characteristic which can be used to predict the rock's failure features and obtain some mechanical properties such as sawability [25], drillability [26], TBM penetration rate [27], and fracture toughness [28], it is of great significance to give more attention to the variation of shale brittleness after fluid-rock interactions.

The accurate evaluation of brittleness is of great importance to drilling and fracturing efficiency. However, expressions to define rock brittleness are various [29, 30]. Considering all the proposed definitions, brittleness can be calculated by three categories: (1) stress-strain curve-based approach. This approach can be used to quantify the brittleness based on the values from the curve, such as strain [31], Young's modulus and Poisson's ratio [32], and energy balance [33]. (2) Strength tests and impact or hardness test approach. Based on some simple laboratory tests, some values like strength [34], degree of impact [35], and hardness [36] show accurate calculating results of rock brittleness [26, 31]. (3) Mineral composition approach. The content of brittle minerals [37], porosity [38], and grain size distribution [39] have been proved to have close relationships to rock brittleness.

In this study, brittleness variations of shale samples which adsorbed in sub/supercritical CO_2 + NaCl fluids with different times were investigated by conducting a series of uniaxial compressive strength (UCS) tests. The statistical damage constitutive model together with the energy-based method was applied to obtain the influence of the difference of soaking condition and soaking time on shale's brittleness.

2. Theoretical and Empirical Equations for Brittleness Index Calculation

The stress-strain-based calculation, which consists of a strain-based method, Young's modulus-based method, Poisson's ratio-based method, and energy-based method, is commonly used in brittleness evaluation [29]. As the compression process of a rock presents a balance between energy storage and consumption, the energy-based method is chosen for the brittleness evaluation in this study. The key issue for the energy-based method is to obtain the relationship between stress and strain. The statistical damage constitutive model is a well-known method to establish the stress-strain relations which considers the anisotropy of rocks. Therefore, in this study, the brittleness of shale samples is calculated by energy-based method together with the statistical damage constitutive model.

2.1. Statistical Damage Constitutive Models of Rocks under Uniaxial Tests. There are four common distributions which have been used in rock mechanics: power function distribution [40], Weibull distribution [41], normal distribution [42], and normal logarithmic distribution [43]. According to Wu et al. [30], the power function distribution and Weibull distribution are chosen to model the stress-strain curves of shale samples.

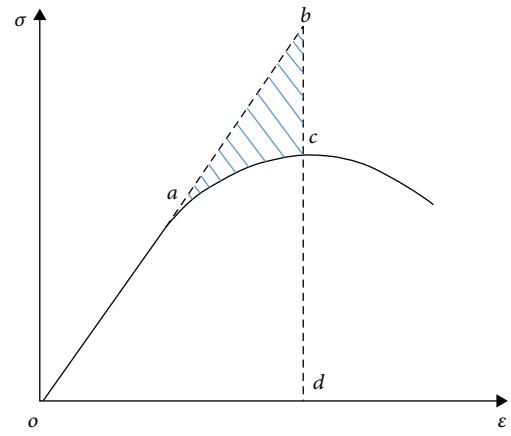

Figure 1: Energy evolution during compression.

Based on the strain equivalent principle [44] and the Hooke's law, the relationship between stress and strain can be described as follows:

$$\sigma = E\varepsilon(1 - D). \tag{1}$$

The damage variable is calculated from (1),

$$D = 1 - \frac{\sigma}{E\varepsilon}, \tag{2}$$

where σ is axial stress, E is Young's modulus, ε is axial strain, and D is damage variable.

In the statistical model, we define the total number of microunit as N, the failed units at a certain loading as n. Then, damage variable is calculated as

$$D = \frac{n}{N}. \tag{3}$$

The number of failed units can be calculated by the following equation,

$$n = N\int_0^{\varepsilon_1} P(\varepsilon)d\varepsilon, \tag{4}$$

where $P(\varepsilon)$ is the distribution function of microstrength, which can be replaced by axial strain ε, and ε_1 is the axial strain at a certain loading.

The probability density function for power function distribution and Weibull distribution are as follows:

$$\begin{aligned} P(\varepsilon) &= \frac{m}{\varepsilon_0}\left(\frac{\varepsilon}{\varepsilon_0}\right)^{m-1}, \\ P(\varepsilon) &= \frac{m}{\varepsilon_0}\left(\frac{\varepsilon}{\varepsilon_0}\right)^{m-1}\exp\left[-\left(\frac{\varepsilon}{\varepsilon_0}\right)^{m}\right], \end{aligned} \tag{5}$$

where m and ε_0 are distribution parameters.

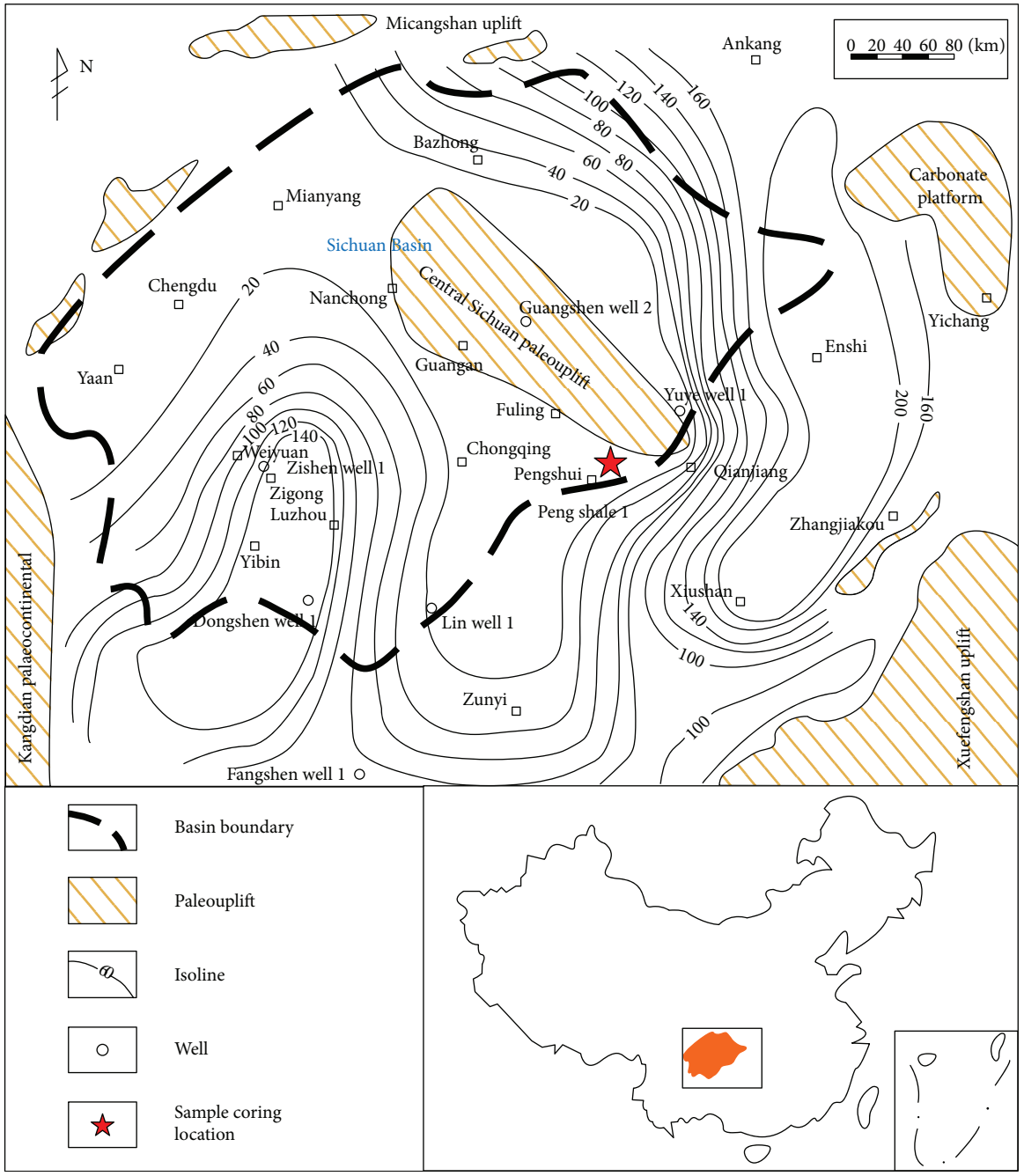

Figure 2: A sketch map of Longmaxi shale in Sichuan Basin, China.

Considering the fact that damage variable is zero when the compression is in the elastic stage, a threshold value of axial strain λ is adopted in the model. The value of λ varies between 0.7 and 0.9 times of axial strain at failure point [45]. This can be described as follows:

$$D = \begin{cases} \int_0^{\lambda} P(\varepsilon)d\varepsilon = 0, & \varepsilon < \lambda, \\ \int_{\lambda}^{\varepsilon_1} P(\varepsilon)d\varepsilon, & \varepsilon \geq \lambda. \end{cases} \tag{6}$$

Therefore, the probability density function for the two distributions is rewritten as follows:

$$P(\varepsilon) = \frac{m}{\varepsilon_0}\left(\frac{\varepsilon - \lambda}{\varepsilon_0}\right)^{m-1}, \quad P(\varepsilon) = \frac{m}{\varepsilon_0}\left(\frac{\varepsilon - \lambda}{\varepsilon_0}\right)^{m-1} \exp\left[-\left(\frac{\varepsilon - \lambda}{\varepsilon_0}\right)^{m}\right]. \tag{7}$$

Combined the previous equations, the statistical damage constitutive models based on power function distribution and Weibull distribution can be obtained as follows:

$$\sigma = \begin{cases} E\varepsilon, & \varepsilon < \lambda, \\ E\varepsilon\left[1 - \left(\dfrac{\varepsilon - \lambda}{\varepsilon_0}\right)^m\right], & \varepsilon \geq \lambda, \end{cases}$$
$$\sigma = \begin{cases} E\varepsilon, & \varepsilon < \lambda, \\ E\varepsilon \exp\left[-\left(\dfrac{\varepsilon - \lambda}{\varepsilon_0}\right)^m\right], & \varepsilon \geq \lambda. \end{cases} \tag{8}$$

In view of the extreme point at the stress-strain curve, the two constitutive models should fulfil the following equation:

$$\begin{aligned} \sigma &= \sigma_{\max}, \\ \varepsilon &= \varepsilon_{\max}, \\ \frac{d\sigma_{\max}}{d\varepsilon_{\max}} &= 0, \end{aligned} \tag{9}$$

where $\sigma_{\max}$ the axial stress at failure point and $\varepsilon_{\max}$ the axial strain at failure point.

Then, the two distribution parameters can be calculated by (10) for power function distribution and (11) for Weibull distribution.

$$\begin{aligned} m &= \frac{\sigma_{\max}(\varepsilon_{\max} - \lambda)}{\varepsilon_{\max}(E\varepsilon_{\max} - \sigma_{\max})}, \\ \varepsilon_0 &= \frac{\varepsilon_{\max} - \lambda}{\left((E\varepsilon_{\max} - \sigma_{\max})/E\varepsilon_{\max}\right)^{1/m}}, \end{aligned} \tag{10}$$

$$\begin{aligned} m &= \frac{\varepsilon_{\max} - \lambda}{\varepsilon_{\max}\ln(E\varepsilon_{\max}/\sigma_{\max})}, \\ \varepsilon_0 &= \frac{\varepsilon_{\max} - \lambda}{\left((\varepsilon_{\max} - \lambda)/m\varepsilon_{\max}\right)^{1/m}}. \end{aligned} \tag{11}$$

2.2. Energy Method for Brittleness Calculation. The statistical damage constitutive models could only obtain accurate stress-strain relations in the prepeak stage. Therefore, we only use the energy before the peak point to calculate the brittleness in this study. The energy balance during compression is shown in Figure 1. The area of S_{oabd} means the elastic energy during compression; the area of S_{oacd} means the energy stored in the rock during compression; the area of S_{abc} means the energy consumed in the compression [46]. The lower the value of S_{abc} is, the more brittle the rock is. If $S_{abc} = 0$, the rock will be a kind of ideal brittle material.

The elastic energy of rock before failure is

$$S_{oabd} = \frac{1}{2}E\varepsilon_{\max}^2. \tag{12}$$

The stored energy before failure is

$$S_{oacd} = \int_0^{\varepsilon_{\max}} \sigma d\varepsilon. \tag{13}$$

The brittleness index (BI) is defined as the ratio of stored energy and elastic energy, which is

Table 1: Mineralogy of shale samples (the samples are cored from the same place as mentioned before [17, 24]).

X-ray diffraction analysis	Value (%, *w*/*w*)
Brittleness component (total)	72.95
Quartz	55.50
Feldspar	14.57
Cristobalite	2.88
Clay component (total)	5.85
Kaolinite	1.00
Illite	1.42
Smectite	3.43
Others (total)	20.97
Pyrite	4.08
Calcite	4.44
Muscovite	5.57
Annite	1.41
Marble	5.10
Braunite	0.37

Table 2: The soaking arrangement of shale samples.

Condition	Group number	Temperature (°C)	Pressure (MPa)	Time (day)
Intact	1	22	—	—
Subcritical CO_2 + NaCl	2	40	7	10
	3	40	7	20
	4	40	7	30
Supercritical CO_2 + NaCl	5	40	9	10
	6	40	9	20
	7	40	9	30

$$\mathrm{BI} = \frac{S_{oacd}}{S_{oabd}} = \frac{2\int_0^{\varepsilon_{\max}}\sigma d\varepsilon}{E\varepsilon_{\max}^2} = \frac{E\lambda^2 + 2\int_\lambda^{\varepsilon_{\max}}\sigma d\varepsilon}{E\varepsilon_{\max}^2}. \tag{14}$$

Combined the constitutive models and BI equation, the final equation of BI with power function distribution is shown in (15) and Weibull distribution is shown in (16).

$$\begin{aligned} \mathrm{BI} &= \frac{E\lambda^2 + 2\int_\lambda^{\varepsilon_{\max}} E\varepsilon[1 - ((\varepsilon - \lambda)/\varepsilon_0)^m]\, d\varepsilon}{E\varepsilon_{\max}^2} \\ &= 1 - \frac{2(\varepsilon_{\max} - \lambda)^{m+1}}{\varepsilon_{\max}^2\varepsilon_0^m}\left(\frac{\varepsilon_{\max} - \lambda}{m+2} + \frac{\lambda}{m+1}\right), \end{aligned} \tag{15}$$

$$\mathrm{BI} = \frac{E\lambda^2 + 2\int_\lambda^{\varepsilon_{\max}} E\varepsilon \exp[-((\varepsilon - \lambda)/\varepsilon_0)^m]\, d\varepsilon}{E\varepsilon_{\max}^2}. \tag{16}$$

3. Experimental Methodology and Results

3.1. Sample Preparation. Shale samples used in this study were Longmaxi shale obtained from Sichuan Basin, China, as shown in Figure 2 [11]. The shales in these areas are characterized as having high thickness, suitable burial depth, and effective fracture development [47]. Samples were cored from a slightly weathered outcrop sample. XRD tests were

Table 3: Values of uniaxial compressive strength (UCS) and Young's modulus (E) for all tested samples.

Specimen		UCS (MPa)	Average UCS (MPa) Standard deviation (MPa)	ΔUCS	Young's modulus (GPa)	Average E (GPa) Standard deviation (GPa)	ΔE
Intact	Number 1	50.27	53.30	—	6.91	6.47	—
	Number 2	56.33	(3.03)		6.02	(0.45)	
				10 days			
Subcritical CO_2 + NaCl	Number 1	40.98	42.22	−20.79%	5.48	5.62	−13.14%
	Number 2	43.46	(1.24)		5.75	(0.14)	
				20 days			
	Number 1	31.61	34.15	−35.93%	4.23	4.45	−31.22%
	Number 2	36.69	(2.54)		4.67	(0.22)	
				30 days			
	Number 1	20.57	23.03	−56.79%	2.48	2.67	−58.73%
	Number 2	25.49	(2.46)		2.86	(0.19)	
				10 days			
	Number 1	36.15	37.75	−29.17%	4.60	4.79	−25.97%
	Number 2	39.34	(1.60)		4.97	(0.19)	
	Number 3	11.89	Excluded		0.93		
				20 days			
Supercritical CO_2 + NaCl	Number 1	24.50	25.28	−52.57%	2.89	3.03	−53.17%
	Number 2	26.06	(0.78)		3.16	(0.13)	
				30 days			
	Number 1	18.90	20.51	−61.52%	2.06	2.43	−62.44%
	Number 2	22.11	(1.61)		2.79	(0.37)	
	Number 3	12.33	Excluded		1.16		

performed on a Bruker AXS D8-Focus X-ray diffractometer at the Institute of Rock and Soil Mechanics, Chinese Academy of Sciences, Wuhan, China, as shown in Table 1. It can be seen that the shale sample has a high percentage of brittle minerals (72.95%) and a low percentage of clay contents (5.85%), which means that the shale formation has good fracture performance. The samples were cored parallel to bedding; based on the ASTM standards, owing to a <10% coring success rate of the shale limited samples was available. The coring process may have created some microfractures. Samples used in the study were selected carefully from all cored samples to ensure good quality. The size of the samples was Φ30 mm × 60 mm. The experiments were conducted at the 3G Deep Earth Lab, Monash University, Australia.

3.2. Testing Arrangement. Samples were firstly divided into seven groups. Each group had two samples. Six groups were soaked in subcritical/supercritical CO_2 with NaCl solution for different times (10 days, 20 days, and 30 days). The group with no imbibition (intact) was set as the control group. The concentration of NaCl solution was 20% by weight. The soaking arrangement was listed in Table 2. If the compression results of one group have large deviations, additional tests will be done until the results are acceptable.

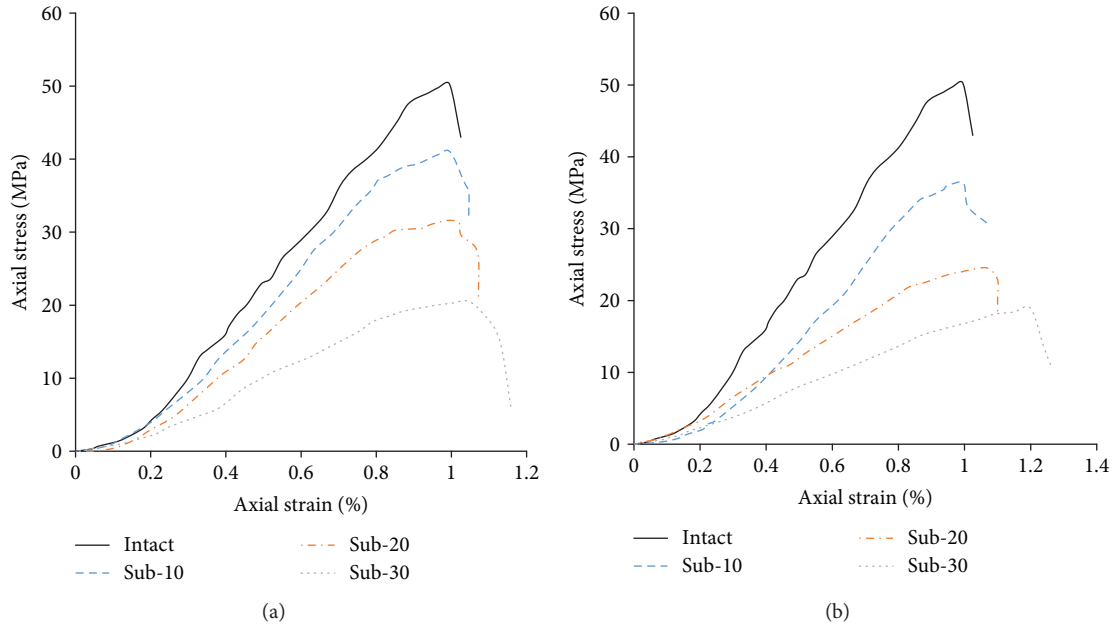

Figure 3: The axial stress-axial strain curves for intact sample and samples with subcritical CO_2 + NaCl solution (a) and supercritical CO_2 + NaCl solution (b). "Sub-10" means samples soaked in subcritical CO_2 and NaCl for 10 days. "Sup-10" means samples soaked in supercritical CO_2 and NaCl for 10 days.

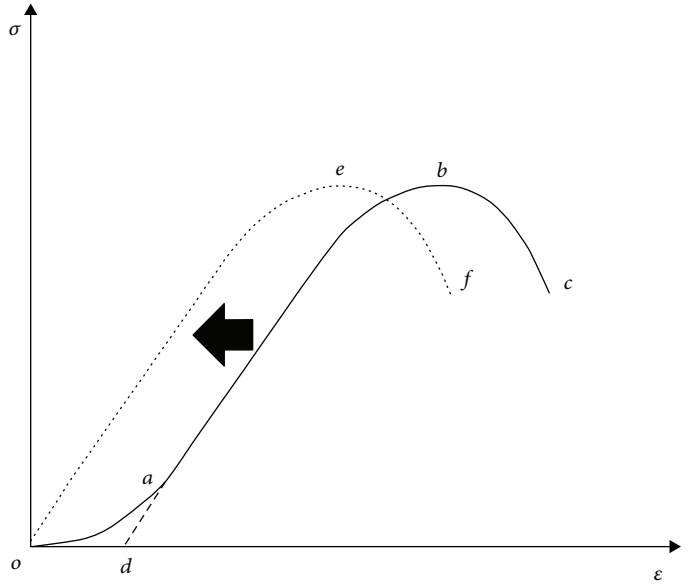

Figure 4: The transformation of the stress-strain curves.

The soaking pressure was controlled by a Model 500D pump with a precision of 1 kPa. The temperature was offered by an electrical cover with a precision of 1°C. After imbibition, CO_2 in the high-pressure chamber was drained very slowly to keep the pressure dropped smoothly. Then, samples were taken out and placed in the air for 24 hours to eliminate high pore pressure. Before the compression tests, all shale samples were painted with white and black paintings to make sure that the lateral surface can be recognized by ARAMIS digital cameras. All the UCS tests were conducted in a Shimadzu AG 9300 kN compression machine with a loading rate of 0.10 mm/min. The axial and lateral strains of tested samples were recorded by a 3D ARAMIS digital equipment.

3.3. Experimental Results. The UCS values and Young's modulus of tested samples were listed in Table 3. For each group, only one sample's stress-strain curve was presented in this study for analysis and brittleness calculation.

The axial stress-axial strain curves for samples soaked with subcritical CO_2 and NaCl are shown in Figure 3(a). It can be seen that, for shale samples soaked in subcritical

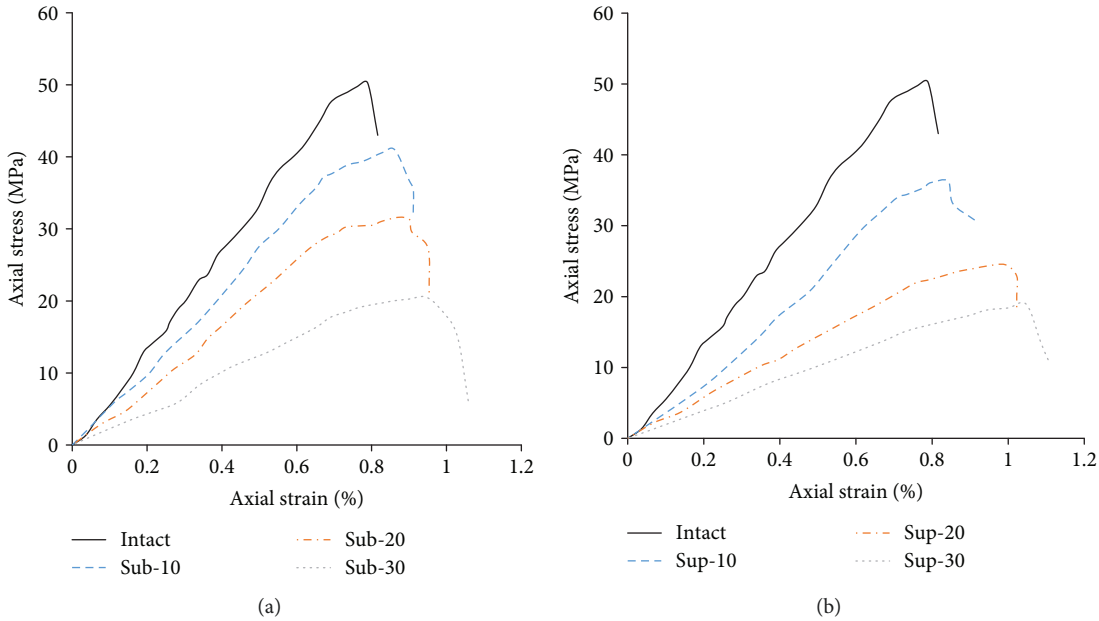

Figure 5: The transformed axial stress-axial strain curves without a crack closure stage. (a) Intact samples and samples with subcritical CO_2 + NaCl solution. (b) Intact samples and samples with supercritical CO_2 + NaCl solution.

Table 4: The mechanical values of shales obtained from stress-strain curves.

Condition	Soaking time (day)	Peak axial stress (MPa)	Axial strain at failure point (%)	Young's modulus (GPa)	Axial strain (%)		
					$\lambda = 0.7$	$\lambda = 0.8$	$\lambda = 0.9$
Intact	—	50.27	0.789	6.91	0.552	0.631	0.710
Subcritical CO_2 + NaCl	10	40.98	0.862	5.48	0.603	0.690	0.776
	20	31.61	0.872	4.23	0.610	0.698	0.785
	30	20.57	0.943	2.48	0.660	0.754	0.849
Supercritical CO_2 + NaCl	10	36.15	0.842	4.60	0.589	0.674	0.758
	20	24.50	0.993	2.89	0.695	0.794	0.894
	30	18.90	1.048	2.06	0.734	0.838	0.943

CO_2 + NaCl solution for 10 days, the UCS values and Young's modulus show reductions of 20.79% and 13.14%, respectively. While extending the soaking time to 20 and 30 days, the reductions of UCS and Young's modulus become larger. However, the axial strain at the failure point increases with increasing soaking time. Figure 3(b) shows the axial stress-axial strain curves for samples under supercritical CO_2 and NaCl imbibition. The variation trends of UCS and Young's modulus values are similar to samples soaked in subcritical CO_2 + NaCl solution. According to the previous study [11], the change of shale's mechanical properties is because of the physical and chemical reactions during the imbibition. Therefore, it is necessary to manifest the effect of such physical and chemical reactions on shale's brittleness, which is of great importance for formation fracturing. When the soaking time is the same, the values of UCS and Young's for samples soaked in supercritical condition are smaller than that soaked in subcritical condition. Whether the difference of soaking condition will influence shale's brittleness is also need to be studied.

4. Brittleness Calculation and Discussion

4.1. Models' Calculation and Validation. A complete stress-strain curve contains five stages: crack closure stage, elastic stage, stable crack propagation stage, unstable crack propagation stage, and postpeak stage [48, 49]. The statistical damage constitutive models cannot correctly present the crack closure and postpeak stages. Therefore, the axial stress-axial strain curves in this study have been transformed to eliminate the crack closure stage. The transformation is made by inversely extending the line in the elastic stage and obtaining the intersection point with x-axis, then making a leftward shift of the curve *dabc* to let the point d move to the origin coordinate and a new curve *oef* is obtained, as shown in Figure 4. Finally, the new axial stress-axial strain curves for intact and soaked samples are shown in Figure 5. For each group (see Table 2), only one sample is chosen to do the calculation. The peak axial stress, the axial strain at failure point, Young's modulus, and the axial strain with different threshold values are listed in Table 4.

Table 5: Distribution parameters of intact and soaked samples.

Soaking condition			Intact	Subcritical CO_2 + NaCl			Supercritical CO_2 + NaCl		
Soaking time (day)			—	10	20	30	10	20	30
$\lambda = 0.7$	Power	m	3.5486	1.9647	1.7975	2.1911	4.2002	1.751	2.1087
		ε_0	0.1517	0.0807	0.0693	0.0959	0.1745	0.0649	0.0909
	Weibull	m	3.6965	2.1111	1.9437	2.3379	4.3485	1.897	2.2554
		ε_0	0.2326	0.3384	0.3688	0.3426	0.2391	0.4303	0.3906
$\lambda = 0.8$	Power	m	2.3657	1.3098	1.1983	1.4607	2.8002	1.1673	1.4058
		ε_0	0.0809	0.0301	0.0238	0.0372	0.0967	0.0202	0.0326
	Weibull	m	2.4644	1.4074	1.2958	1.5586	2.899	1.2647	1.5036
		ε_0	0.3154	0.6365	0.7417	0.5976	0.3049	0.8833	0.6991
$\lambda = 0.9$	Power	m	1.1829	0.6549	0.5992	0.7304	1.4001	0.5837	0.7029
		ε_0	0.0208	0.0026	0.0016	0.0037	0.0278	0.001	0.0025
	Weibull	m	1.2322	0.7037	0.6479	0.7793	1.4495	0.6323	0.7518
		ε_0	0.2459	1.3985	2.0432	1.0242	0.1978	2.6129	1.3028

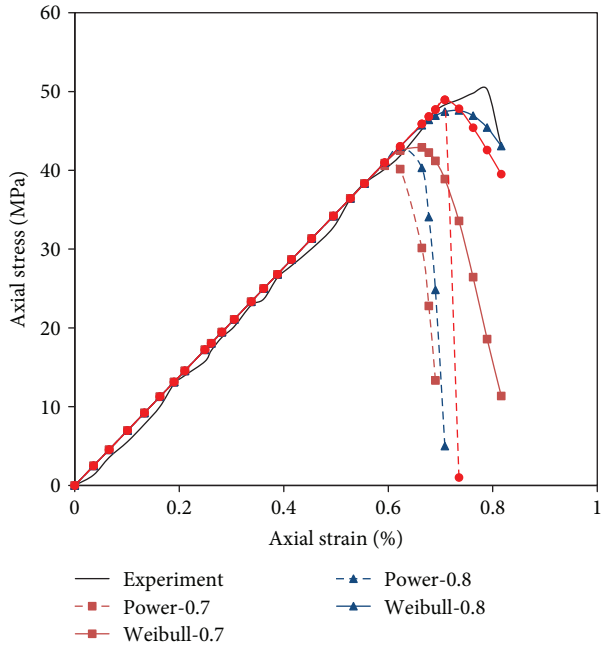

Figure 6: Experimental and constitutive modelling axial stress-axial strain curves of the intact sample.

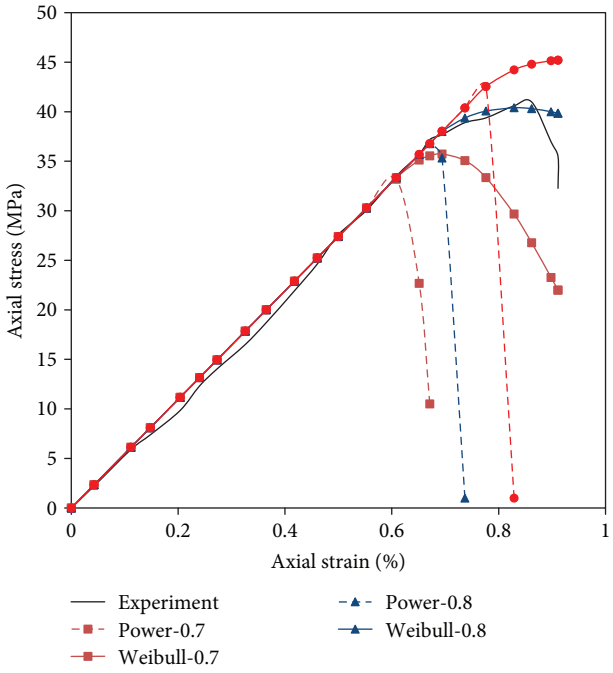

Figure 7: Experimental and constitutive modelling axial stress-axial strain curves of the sample soaked in subcritical CO_2 for 10 days.

When substituting the values in Table 4 into (10) and (11), we can obtain the values of the two distribution parameters: m and ε_0, as shown in Table 5. In order to manifest the influence of threshold value on the variations between experimental results and constitutive modelling results, the axial stress-axial strain relations of the intact sample and samples soaked in subcritical/supercritical CO_2 for 10 days are calculated based on the power function distribution and Weibull distribution, which are shown in Figures 6–8, respectively.

According to Figures 6–8, we can see that stress-strain curves obtained by power function distribution-based constitutive model have very steep trends around the failure points, while the curves calculated by Weibull distribution-based constitutive model present gradual trends around the failure points, which are closely related to the experimental results. It can be deduced that Weibull distribution can better present the stress-strain relations of shale samples than the power function distribution. Before the unstable crack propagation stage, Weibull distribution-based constitutive model presents the same stress-strain relations for the three threshold values. After that, the influence of threshold values on the stress-strain curves occurs. More specifically, the highest threshold

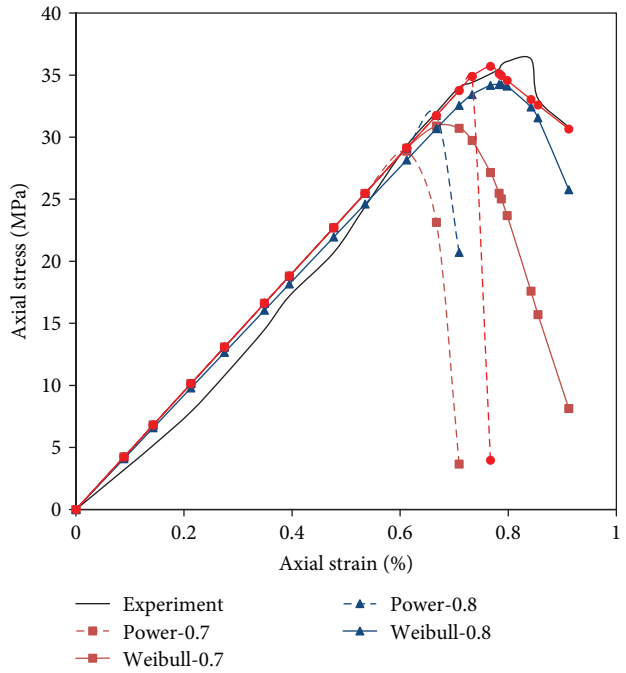

Figure 8: Experimental and constitutive modelling axial stress-axial strain curves of the sample soaked in supercritical CO_2 for 10 days.

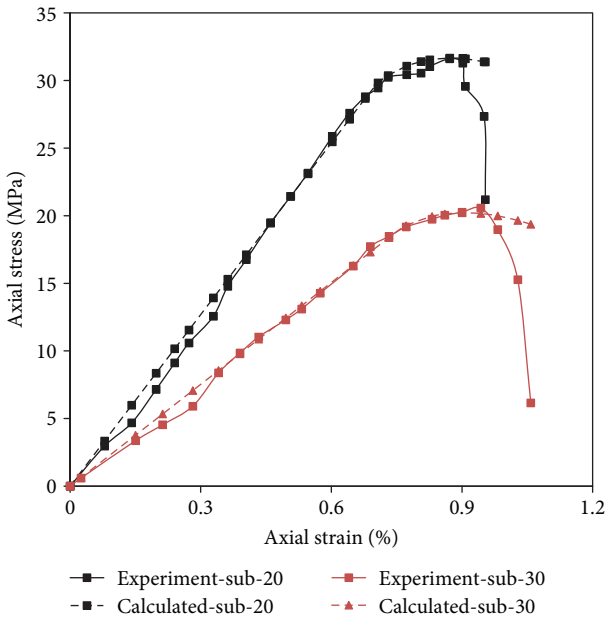

Figure 9: Experimental and constitutive model calculated stress-strain curves for samples soaked in subcritical CO_2 for 20 and 30 days.

value ($\lambda = 0.9$) leads to the overestimated results of stress-strain relationship at the unstable crack propagation stage; the lowest one ($\lambda = 0.7$) causes the underestimated results of stress-strain relationship, while the moderate threshold value ($\lambda = 0.8$) presents good stress-strain relationship for

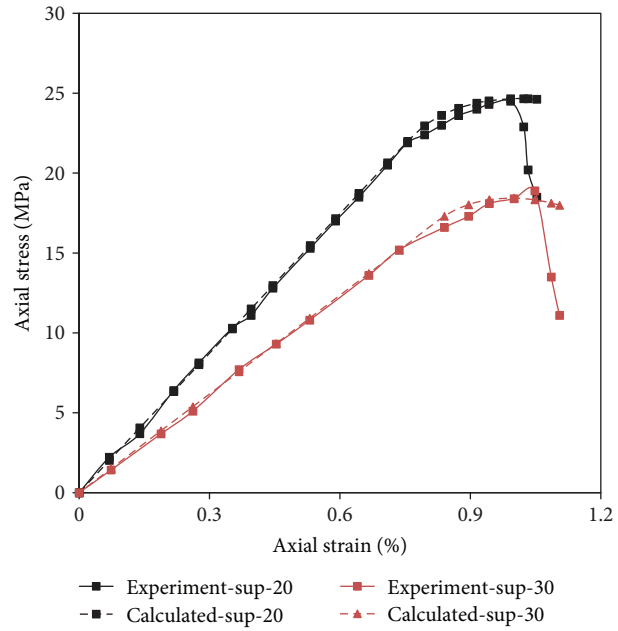

Figure 10: Experimental and constitutive model calculated stress-strain curves for samples soaked in supercritical CO_2 for 20 and 30 days.

the three kinds of samples. Therefore, in this study, the Weibull distribution-based constitutive model with a threshold value of 0.8 is chosen to calculate the brittleness values of samples with/without imbibition.

The experimental and model calculated stress-strain curves for samples soaked in subcritical CO_2 + NaCl solution and supercritical CO_2 + NaCl solution with 20 and 30 days are shown in Figures 9 and 10, respectively. It is clear that the Weibull distribution-based constitutive model with a damage threshold value of 0.8 could obtain excellent stress-strain relationship for intact and soaked shale samples. Compared to the experimental results, the constitutive model can only acquire good stress-strain results before the failure point. This is true that the constitutive model is infeasible for the postpeak stage. Weibull distribution-based damage constitutive equations for samples with different soaking conditions are listed in Table 6.

4.2. Brittleness Calculation. Weibull distribution-based damage constitutive equations for samples with different soaking conditions are substituted into (16). The quad integration method is applied to calculate the brittleness index of shale samples. The BI values of the intact sample and soaked samples are shown in Table 7. Variations of BI values versus soaking time are shown in Figure 11.

According to Table 7 and Figure 11, all the shale samples have ultra-high BI values which vary from 0.9713 to 0.9961. More specifically, the intact shale sample has the highest BI value of 0.9961. BI values show minor reductions for all soaked samples when compared to intact samples. When the imbibition times are 10 days, 20 days, and 30 days, the B I values are 0.9843, 0.9754, and 0.9851 for samples absorbed in subcritical CO_2 + NaCl solutions and 0.9757, 0.9713, and

Table 6: The Weibull distribution based damage constitutive equations of all samples.

Soaking time (day)	Soaking condition: Subcritical CO_2 + NaCl	Soaking condition: Supercritical CO_2 + NaCl
0	$\sigma = \begin{cases} 6.91 * 10 * \varepsilon, \varepsilon < 0.631, \\ 6.91 * 10 * \varepsilon \exp[-((\varepsilon - 0.631)/0.3154)^{2.4644}], \varepsilon \geq 0.631 \end{cases}$	
10	$\sigma = \begin{cases} 5.48 * 10 * \varepsilon, \varepsilon < 0.690, \\ 5.48 * 10 * \varepsilon \exp[-((\varepsilon - 0.690)/0.6365)^{1.4074}], \varepsilon \geq 0.690 \end{cases}$	$\sigma = \begin{cases} 4.60 * 10 * \varepsilon, \varepsilon < 0.674, \\ 4.60 * 10 * \varepsilon \exp[-((\varepsilon - 0.674)/0.3049)^{2.8990}], \varepsilon \geq 0.674 \end{cases}$
20	$\sigma = \begin{cases} 4.23 * 10 * \varepsilon, \varepsilon < 0.698, \\ 4.23 * 10 * \varepsilon \exp[-((\varepsilon - 0.698)/0.7417)^{1.2958}], \varepsilon \geq 0.698 \end{cases}$	$\sigma = \begin{cases} 2.89 * 10 * \varepsilon, \varepsilon < 0.794, \\ 2.89 * 10 * \varepsilon \exp[-((\varepsilon - 0.794)/0.8833)^{1.2647}], \varepsilon \geq 0.794 \end{cases}$
30	$\sigma = \begin{cases} 2.51 * 10 * \varepsilon, \varepsilon < 0.754, \\ 2.51 * 10 * \varepsilon \exp[-((\varepsilon - 0.754)/0.6826)^{1.4251}], \varepsilon \geq 0.754 \end{cases}$	$\sigma = \begin{cases} 2.06 * 10 * \varepsilon, \varepsilon < 0.838, \\ 2.06 * 10 * \varepsilon \exp[-((\varepsilon - 0.838)/0.6991)^{1.5036}], \varepsilon \geq 0.838 \end{cases}$

Table 7: The brittleness index (BI) of intact samples and soaked samples.

Soaking condition	Soaking time (day)	BI (%)	ΔBI (%)
Intact	—	0.9961	—
Subcritical CO_2 + NaCl	10	0.9843	1.18
	20	0.9754	2.08
	30	0.9851	1.10
Supercritical CO_2 + NaCl	10	0.9757	2.05
	20	0.9713	2.49
	30	0.9835	1.26

0.9835 for samples absorbed in supercritical CO_2 + NaCl solution, respectively. The minimum BI values for the two kinds of soaking solutions are occurred when the imbibition time is 20 days. When extending the soaking time to 30 days, the BI values increase. Meanwhile, the supercritical condition creates a higher reduction of the BI value than that of subcritical condition when the soaking time is the same.

4.3. Discussion. The high value of BI for the intact shale sample is in accordance with the XRD results that shale samples in this study have a high percentage of brittleness minerals. As the loading direction is parallel to the bedding, the sample will reach to its failure point at a sudden and the consumed energy during the compression is very small. Therefore, the compression of the intact shale sample is close to an ideal brittle failure process. Figure 12 shows the lateral strain distribution of the intact shale sample at failure point. It can be seen that before the failure, a large crack has been formed through the sample which is parallel to the beddings. The strain variations for other places are very small, which means the stress is concentrated on the main load-bearing beddings. When the load-bearing beddings are broken, the shale sample fails. Therefore, the stable crack propagation stage and the unstable crack propagation stage are very short which result in a very high BI value.

The reductions of brittleness for soaked shale samples are mainly caused by the chemical reactions during the imbibition. According to the authors' previous work, the pH of

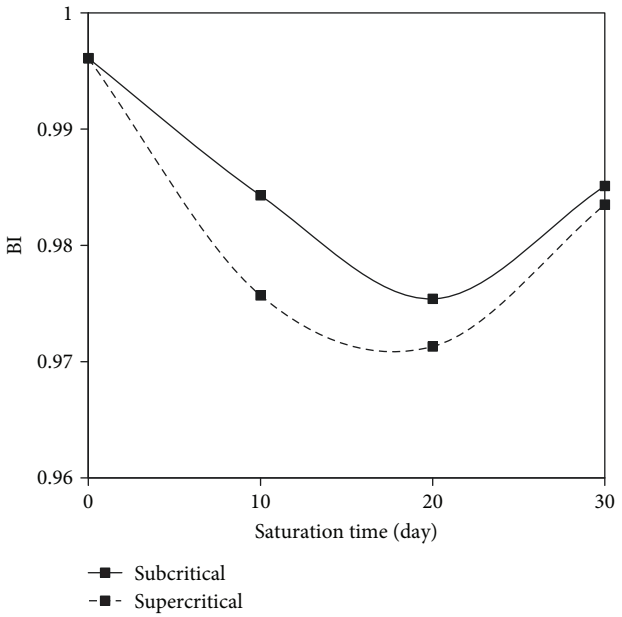

Figure 11: The variation of BI values with soaking time.

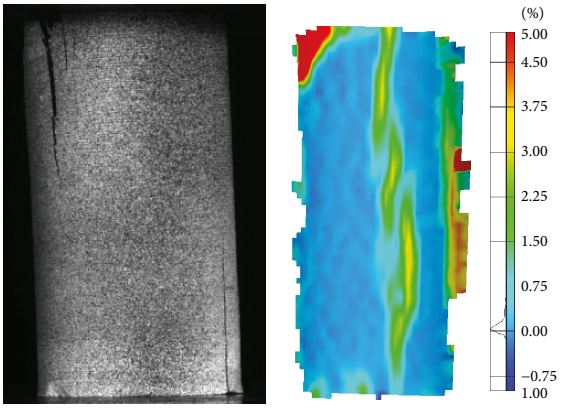

Figure 12: The intact shale sample (a) and the corresponding lateral strain distribution (b).

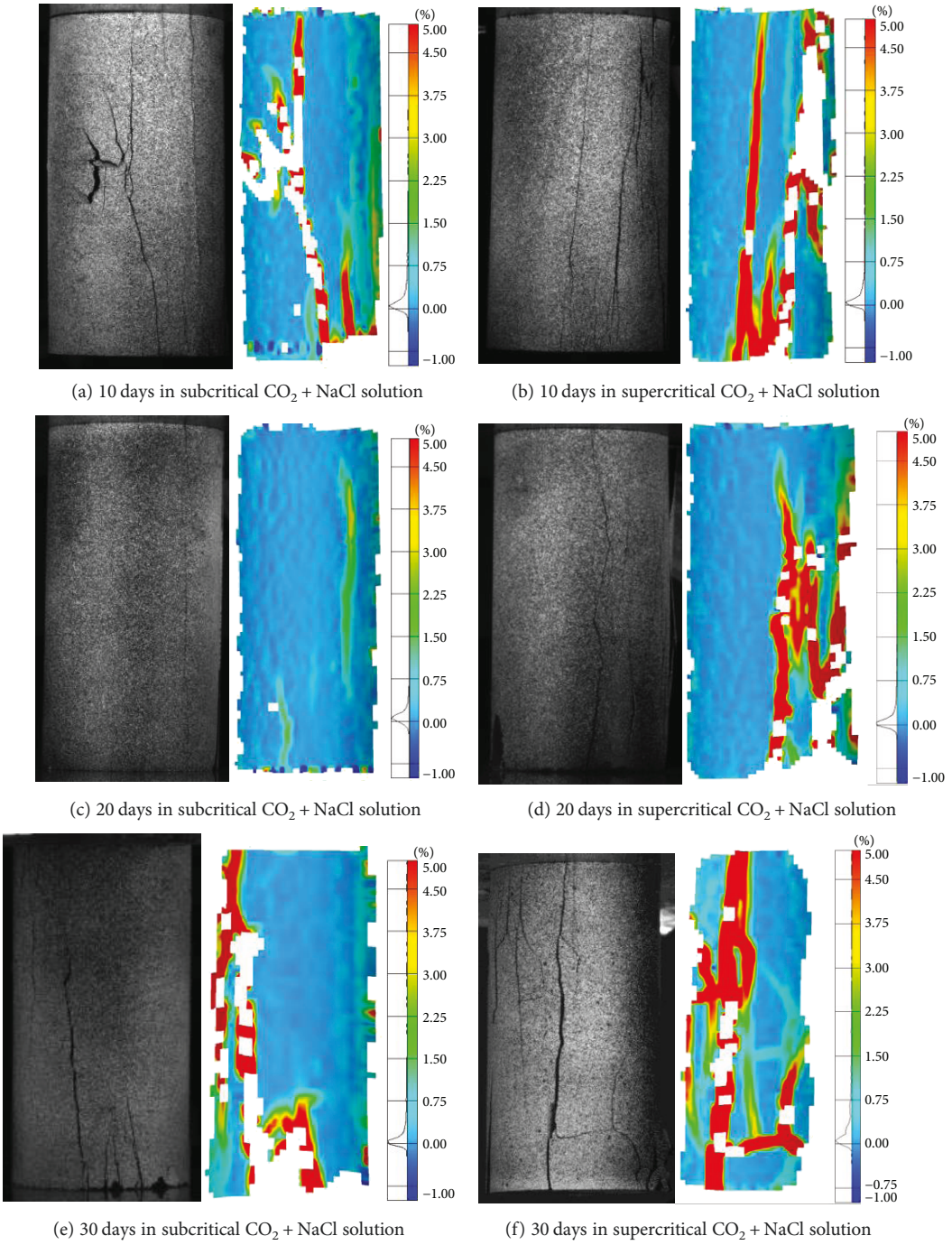

(a) 10 days in subcritical CO_2 + NaCl solution

(b) 10 days in supercritical CO_2 + NaCl solution

(c) 20 days in subcritical CO_2 + NaCl solution

(d) 20 days in supercritical CO_2 + NaCl solution

(e) 30 days in subcritical CO_2 + NaCl solution

(f) 30 days in supercritical CO_2 + NaCl solution

Figure 13: The lateral strain distribution of soaked shale samples. (a), (c), and (e) are in subcritical CO_2 + NaCl solution; (b), (d), and (f) are in supercritical CO_2 + NaCl solution.

water soaked with subcritical and supercritical CO_2 under the same pressure and temperature will be smaller than 3 [11]. The acid fluid will lead to the dissolution and precipitation of some minerals, such as K-feldspar, carbonates, some clay minerals, and iron-containing minerals. The chemical reactions will create pores and enlarge cracks which decrease shale's strength and Young's modulus. The soaked shale samples will become more ductile, and the brittleness values decrease. Figure 13 presents the lateral strain distributions of the soaked samples. Compared to the strain distribution of the intact sample in Figure 12, soaked shale samples have more macroscopic cracks on the surfaces when samples reach their failure points. This difference is also caused by pores and cracks created by chemical reactions. Samples soaked in supercritical CO_2 + NaCl solution present lower B I values than that soaked in subcritical CO_2 + NaCl solution when the soaking time is the same. This is because of the difference of soaking pressure and the phase of CO_2. Higher confining pressure will promote the penetration of fluids into the shale and will make the chemical reactions more

sufficiently. Compared to subcritical CO_2, supercritical CO_2 has no capillary force and lower viscosity, which will make it easy to flow into shale samples. As the phase of CO_2 is also related to the pressure, it is difficult to manifest which one has the dominant effect on the difference of BI values. The increase of BI values of shale samples soaked in subcritical/supercritical CO_2 + NaCl solutions from 20 days to 30 days is probably caused by the fact that the increasing speed of precipitation in the last 10 days increases. The crystals appeared in cracks and decrease the ductile of the shale which lead to the increase of brittleness. Overall, the imbibition of shale samples in subcritical/supercritical CO_2 + NaCl solutions has larger effect on shale's strength and Young's modulus than on the brittleness. The fracture performance of this kind of low-clay shale is still good enough after imbibition.

In this paper, because of the limitation of the theory and experiments, a much more precise results of brittleness values for shale samples soaked in different conditions with different times cannot be obtained. Firstly, the crack closure stage is ignored during the modelling and brittleness calculation process. It will influence the brittleness values of shale samples. Meanwhile, samples soaked in subcritical/supercritical CO_2 + NaCl solutions with different times will have different damage threshold values. However, this paper only uses one threshold value ($\lambda = 0.8$) for all statistical damage constitutive equations. More importantly, shale gas exploitation and CCUS are usually last for decades or even longer. Therefore, a much longer imbibition process is of a great significance to manifest the brittleness variation of shales caused by CO_2 capture and sequestration and CO_2-enhanced shale gas exploitation.

5. Conclusions

The damage statistical constitutive model together with the energy-based approach was applied to calculate the brittleness of shale samples soaked in subcritical/supercritical CO_2 + NaCl solutions with different times. Some remarkable conclusions can be obtained as follows.

Physical and chemical reactions during the imbibition in subcritical/supercritical CO_2 + NaCl solutions cause reductions of shales' peak axial strength (20.79%~61.52%) and Young's modulus (13.14%~62.44%). The two values of soaked samples decrease with increasing saturation time. With the same damage threshold value, the Weibull distribution-based model presents better stress-strain results than the power function distribution-based model. For intact and soaked shale samples, the damage threshold value of 0.8 is appropriate to describe the stress-strain relations; lower or higher threshold values will cause the underestimation or overestimation of the peak point on the stress-strain curve.

The energy balance method together with the Weibull distribution based-constitutive model is applied to calculate the brittleness values of samples with or without imbibition. The intact shale sample has the highest BI value of 0.9961. The CO_2-NaCl-shale interactions during the imbibition decrease the brittleness values. The reductions of BI values vary between 1.10% and 2.49%. A 20-day imbibition in subcritical and supercritical conditions results in the lowest BI values among the three soaking durations. Samples in supercritical CO_2 + NaCl solution have lower BI values than that in subcritical CO_2 + NaCl solution when the soaking time is the same.

Subcritical/supercritical CO_2 + NaCl imbibition has higher effect on shale's strength and Young's modulus than on the brittleness. The low-clay shale still keeps good fracture performance after imbibition.

Conflicts of Interest

On behalf of all authors, the corresponding author states that there is no conflict of interests.

Acknowledgments

The authors would like to thank all the technical staffs of the Geomechanics Laboratories at Monash University for their help with the experimental work and the financial support from the National Key Basic Research Program of China (Grant no.: 2014CB239203) and the Innovation-Driven Project of Central South University (Grant no.: 502501005).

References

[1] S. Kouri, E. Tsupari, J. Kärki et al., "The potential for CCUS in selected industrial sectors – summary of concept evaluations in Finland," *Energy Procedia*, vol. 114, pp. 6418–6431, 2017.

[2] Q. Li, Z. A. Chen, J. T. Zhang, L. C. Liu, X. C. Li, and L. Jia, "Positioning and revision of CCUS technology development in China," *International Journal of Greenhouse Gas Control*, vol. 46, pp. 282–293, 2016.

[3] F. Mourits, N. Kulichenko-Lotz, G. H. González, and J. M. Nieta, "Overview of World Bank CCUS program activities in Mexico," *Energy Procedia*, vol. 114, pp. 5916–5932, 2017.

[4] J. F. D. Tapia, J.-Y. Lee, R. E. H. Ooi, D. C. Y. Foo, and R. R. Tan, "Planning and scheduling of CO_2 capture, utilization and storage (CCUS) operations as a strip packing problem," *Process Safety and Environmental Protection*, vol. 104, Part A, pp. 358–372, 2016.

[5] M. Wang and E. Oko, "Special issue on carbon capture in the context of carbon capture, utilisation and storage (CCUS)," *International Journal of Coal Science & Technology*, vol. 4, no. 1, pp. 1–4, 2017.

[6] Y. Du, R. Wang, and H. Ni, "Development of supercritical carbon dioxide drilling and completion experimental system," in *The 4th IEEE Asia-Pacific Power and Energy Engineering Conference*, Shanghai, China, 2012.

[7] J. J. Kolle, "Coiled-tubing drilling with supercritical carbon dioxide," in *SPE/CIM International Conference on Horizontal Well Technology*, Calgary, AB, Canada, 2000, Society of Petroleum Engineers.

[8] H. Wang, G. Li, and Z. Shen, "A feasibility analysis on shale gas exploitation with supercritical carbon dioxide," *Energy Sources, Part A: Recovery, Utilization, and Environmental Effects*, vol. 34, no. 15, pp. 1426–1435, 2012.

[9] R. S. Middleton, J. W. Carey, R. P. Currier et al., "Shale gas and non-aqueous fracturing fluids: opportunities and challenges for supercritical CO_2," *Applied Energy*, vol. 147, pp. 500–509, 2015.

[10] A. Rogala, J. Krzysiek, M. Bernaciak, and J. Hupka, "Non-aqueous fracturing technologies for shale gas recovery," *Physicochemical Problems of Mineral Processing*, vol. 49, no. 1, pp. 313–322, 2013.

[11] Q. Lyu, P. Ranjith, X. Long, and B. Ji, "Experimental investigation of mechanical properties of black shales after CO_2-water-rock interaction," *Materials*, vol. 9, no. 8, p. 663, 2016.

[12] Q. Lyu, P. G. Ranjith, X. Long, Y. Kang, and M. Huang, "A review of shale swelling by water adsorption," *Journal of Natural Gas Science and Engineering*, vol. 27, pp. 1421–1431, 2015.

[13] A. Busch, P. Bertier, Y. Gensterblum et al., "On sorption and swelling of CO_2 in clays," *Geomechanics and Geophysics for Geo-Energy and Geo-Resources*, vol. 2, no. 2, pp. 111–130, 2016.

[14] X. Li, Z. Feng, G. Han et al., "Breakdown pressure and fracture surface morphology of hydraulic fracturing in shale with H_2O, CO_2 and N_2," *Geomechanics and Geophysics for Geo-Energy and Geo-Resources*, vol. 2, no. 2, pp. 63–76, 2016.

[15] M. Asef, *Shale Engineering: Mechanics and Mechanisms*, CRC Press, Hoboken, NJ, USA, 1st edition, 2013.

[16] R. Wong, "Swelling and softening behaviour of La Biche shale," *Canadian Geotechnical Journal*, vol. 35, no. 2, pp. 206–221, 1998.

[17] Q. Lyu, X. Long, P. G. Ranjith, J. Tan, and Y. Kang, "Experimental investigation on the mechanical behaviours of a low-clay shale under water-based fluids," *Engineering Geology*, vol. 233, pp. 124–138, 2018.

[18] B. Bostrom, G. Svano, P. Horsrud, and A. Askevold, "The shrinkage rate of KCL-exposed smectitic North Sea shale simulated by a diffusion model," in *SPE/ISRM Rock Mechanics in Petroleum Engineering*, Trondheim, Norway, 1998, Society of Petroleum Engineers.

[19] P. Horsrud, B. Bostrom, E. F. Sonstebo, and R. M. Holt, "Interaction between shale and water-based drilling fluids: laboratory exposure tests give new insight into mechanisms and field consequences of KCl contents," in *SPE Annual Technical Conference and Exhibition*, New Orleans, LA, USA, 1998, Society of Petroleum Engineers.

[20] Q. Lyu, X. Long, P. Ranjith, and Y. Kang, "Unconventional gas: experimental study of the influence of subcritical carbon dioxide on the mechanical properties of black shale," *Energies*, vol. 9, no. 7, p. 516, 2016.

[21] H. Yin, J. Zhou, X. Xian et al., "Experimental study of the effects of sub- and super-critical CO_2 saturation on the mechanical characteristics of organic-rich shales," *Energy*, vol. 132, pp. 84–95, 2017.

[22] Q. Lyu, X. Long, P. G. Ranjith, J. Tan, Y. Kang, and Z. Wang, "Experimental investigation on the mechanical properties of a low-clay shale with different adsorption times in sub-/super-critical CO_2," *Energy*, vol. 147, pp. 1288–1298, 2018.

[23] S. Zhang, X. Xian, J. Zhou, and L. Zhang, "Mechanical behaviour of Longmaxi black shale saturated with different fluids: an experimental study," *RSC Advances*, vol. 7, no. 68, pp. 42946–42955, 2017.

[24] Q. Lyu, X. Long, R. PG et al., "A laboratory study of geomechanical characteristics of black shales after sub-critical/super-critical CO_2 + brine saturation," *Geomechanics and Geophysics for Geo-Energy and Geo-Resources*, vol. 4, no. 2, pp. 141–156, 2018.

[25] O. Gunaydin, S. Kahraman, and M. Fener, "Sawability prediction of carbonate rocks from brittleness indexes," *Journal of the Southern African Institute of Mining and Metallurgy*, vol. 104, pp. 1–6, 2004.

[26] R. Altindag, "The evaluation of rock brittleness concept on rotary blast hold drills," *Journal of the Southern African Institute of Mining and Metallurgy*, vol. 102, no. 1, pp. 61–66, 2002.

[27] Q. M. Gong and J. Zhao, "Influence of rock brittleness on TBM penetration rate in Singapore granite," *Tunnelling and Underground Space Technology*, vol. 22, no. 3, pp. 317–324, 2007.

[28] S. Kahraman and R. Altindag, "A brittleness index to estimate fracture toughness," *International Journal of Rock Mechanics and Mining Sciences*, vol. 41, no. 2, pp. 343–348, 2004.

[29] D. Zhang, P. G. Ranjith, and M. S. A. Perera, "The brittleness indices used in rock mechanics and their application in shale hydraulic fracturing: a review," *Journal of Petroleum Science and Engineering*, vol. 143, pp. 158–170, 2016.

[30] C. Wu, J. Tuo, L. Zhang et al., "Pore characteristics differences between clay-rich and clay-poor shales of the Lower Cambrian Niutitang Formation in the Northern Guizhou area, and insights into shale gas storage mechanisms," *International Journal of Coal Geology*, vol. 178, Supplement C, pp. 13–25, 2017.

[31] V. Hucka and B. Das, "Brittleness determination of rocks by different methods," *International Journal of Rock Mechanics and Mining Sciences & Geomechanics Abstracts*, vol. 11, no. 10, pp. 389–392, 1974.

[32] A. Jahandideh and B. Jafarpour, "Optimization of hydraulic fracturing design under spatially variable shale fracability," *Journal of Petroleum Science and Engineering*, vol. 138, pp. 174–188, 2016.

[33] B. Tarasov and Y. Potvin, "Universal criteria for rock brittleness estimation under triaxial compression," *International Journal of Rock Mechanics and Mining Sciences*, vol. 59, pp. 57–69, 2013.

[34] R. Altindag and A. Guney, "Predicting the relationships between brittleness and mechanical properties (UCS, TS and SH) of rocks," *Scientific Research and Essays*, vol. 5, no. 16, pp. 2107–2118, 2010.

[35] M. Protodyakonov, "Mechanical properties and drillability of rocks," in *Proceedings of the Fifth Symposium on Rock Mechanics*, pp. 103–118, Minneapolis, MN, USA, 1962, University of Minnesota.

[36] H. Honda and Y. Sanada, "Hardness of coal," *Fuel*, vol. 35, no. 4, pp. 451–461, 1956.

[37] D. M. Jarvie, R. J. Hill, T. E. Ruble, and R. M. Pollastro, "Unconventional shale-gas systems: the Mississippian Barnett Shale of north-central Texas as one model for thermogenic shale-gas assessment," *AAPG Bulletin*, vol. 91, no. 4, pp. 475–499, 2007.

[38] M. Heidari, G. R. Khanlari, M. Torabi-Kaveh, S. Kargarian, and S. Saneie, "Effect of porosity on rock brittleness," *Rock Mechanics and Rock Engineering*, vol. 47, no. 2, pp. 785–790, 2014.

[39] E. Eberhardt, B. Stimpson, and D. Stead, "Effects of grain size on the initiation and propagation thresholds of stress-induced brittle fractures," *Rock Mechanics and Rock Engineering*, vol. 32, no. 2, pp. 81–99, 1999.

[40] H. Li, Y. Lu, L. Zhou, S. Han, and Y. Gou, "A new constitutive model for calculating the loading-path dependent proppant deformation and damage analysis of fracture conductivity," *Journal of Natural Gas Science and Engineering*, vol. 46, pp. 365–374, 2017.

[41] Z.-l. Wang, Y.-c. Li, and J. G. Wang, "A damage-softening statistical constitutive model considering rock residual strength," *Computers & Geosciences*, vol. 33, no. 1, pp. 1–9, 2007.

[42] S.-r. Zhang, X.-h. Wang, C. Wang, R. Song, and H.-y. Huo, "Compressive behavior and constitutive model for roller compacted concrete under impact loading: considering vertical stratification," *Construction and Building Materials*, vol. 151, pp. 428–440, 2017.

[43] A. Tuli, K. Kosugi, and J. W. Hopmans, "Simultaneous scaling of soil water retention and unsaturated hydraulic conductivity functions assuming lognormal pore-size distribution," *Advances in Water Resources*, vol. 24, no. 6, pp. 677–688, 2001.

[44] J. Lemaitre, J. P. Sermage, and R. Desmorat, "A two scale damage concept applied to fatigue," *International Journal of Fracture*, vol. 97, no. 1/4, pp. 67–81, 1999.

[45] Y. Dong, H. Xie, and S. Li, "Continuum damage mechanics constitutive model of concrete under compression," *Engineering Mechanics*, vol. 13, no. 1, pp. 44–53, 1996.

[46] Y. Li, D. Jia, Z. Rui, J. Peng, C. Fu, and J. Zhang, "Evaluation method of rock brittleness based on statistical constitutive relations for rock damage," *Journal of Petroleum Science and Engineering*, vol. 153, pp. 123–132, 2017.

[47] H. Tian, L. Pan, X. Xiao, R. W. T. Wilkins, Z. Meng, and B. Huang, "A preliminary study on the pore characterization of Lower Silurian black shales in the Chuandong Thrust Fold Belt, southwestern China using low pressure N2 adsorption and FE-SEM methods," *Marine and Petroleum Geology*, vol. 48, Supplement C, pp. 8–19, 2013.

[48] K. Pérez Hidalgo and E. Nordlund, "Comparison between stress and strain quantities of the failure–deformation process of Fennoscandian hard rocks using geological information," *Rock Mechanics and Rock Engineering*, vol. 46, no. 1, pp. 41–51, 2013.

[49] E. Eberhardt, D. Stead, B. Stimpson, and R. S. Read, "Identifying crack initiation and propagation thresholds in brittle rock," *Canadian Geotechnical Journal*, vol. 35, no. 2, pp. 222–233, 1998.